Dark spots on Mercury: A distinctive low-reflectance material and its relation to hollows

Zhiyong Xiao,[1,2,3] Robert G. Strom,[1] David T. Blewett,[4] Paul K. Byrne,[5] Sean C. Solomon,[5,6] Scott L. Murchie,[4] Ann L. Sprague,[1] Deborah L. Domingue,[7] and Jörn Helbert[8]

Received 14 August 2012; revised 4 July 2013; accepted 17 July 2013; published 11 September 2013.

[1] Orbital images acquired by the MErcury, Surface, Space ENvironment, GEochemistry, and Ranging (MESSENGER) spacecraft reveal a distinctive low-reflectance material on the surface of Mercury. Such material occurs in small, isolated, and thin surficial units. We term these features "dark spots." Dark spots have the lowest average reflectance yet documented on the planet. In every case observed at sufficiently high resolution, dark spots feature hollows at their centers. Not all hollows, however, are surrounded by a dark spot. Dark spots have been found on low-reflectance smooth plains, intercrater plains, heavily cratered terrain, and impact craters at almost all longitudes on Mercury, but they have not been documented on high-reflectance smooth plains material. Dark spots are one of the youngest endogenic features on Mercury, and some postdate craters with distinctive rays. Sulfides may be the phase responsible for the low albedo of dark spot material. We propose that dark spots form during the initial stages of hollow formation, perhaps in a manner similar to intense outgassing events that feature exit velocities in excess of 100 m/s. Such outgassing could contemporaneously produce a depression that constitutes an embryonic hollow. Under this scenario, dark spot material is subsequently removed or modified by regolith gardening or other surface processes on time scales shorter than the lifetime of the central hollow.

Citation: Xiao, Z., R. G. Strom, D. T. Blewett, P. K. Byrne, S. C. Solomon, S. L. Murchie, A. L. Sprague, D. L. Domingue, and J. Helbert (2013), Dark spots on Mercury: A distinctive low-reflectance material and its relation to hollows, *J. Geophys. Res. Planets*, *118*, 1752–1765, doi:10.1002/jgre.20115.

1. Introduction

[2] Mercury has long been known to have a lower disk-integrated reflectance than the Moon on the basis of early Earth-based observations and Mariner 10 flyby images [e.g., *Veverka et al*., 1988; *Warell*, 2004]. Mariner 10 data showed that Mercury's crust displays a range of reflectances across its surface [e.g., *Murray et al*., 1974; *Robinson and Lucey*, 1997; *Denevi and Robinson*, 2008]. The three flybys of Mercury by the MErcury, Surface, Space ENvironment, GEochemistry, and Ranging (MESSENGER) spacecraft [*Solomon et al*., 2001] confirmed an earlier finding that the reflectance of immature material on Mercury is typically 10%–20% lower than that of immature material in the lunar highlands, indicating that low-reflectance materials are present in Mercury's crust [*McClintock et al*., 2008; *Robinson et al*., 2008; *Blewett et al*., 2009; *Denevi et al*., 2009].

[3] Two primary types of spectral units with a reflectance lower than the global average were identified on Mercury from observations made during the MESSENGER flybys [*Robinson et al*., 2008; *Denevi et al*., 2009]. The first unit is a subcategory of smooth plains, represented by the plains exterior to the Caloris basin [*Denevi et al*., 2009, 2013]. These plains have a reflectance ~15% lower than the global average, and their reflectance increases with increasing wavelength from visible to near-infrared wavelengths less steeply than does the global average spectrum (i.e., the spectra are "bluer"). These plains have been termed "low-reflectance blue plains" or LBP [*Denevi et al*., 2009]. LBP material occurs around impact craters and basins and may have been emplaced through either volcanic or impact processes [*Strom et al*., 2008; *Fassett et al*., 2009; *Denevi et al*., 2009, 2013].

Additional supporting information may be found in the online version of this article.

[1]Lunar and Planetary Laboratory, University of Arizona, Tucson, Arizona, USA.
[2]Faculty of Earth Sciences, China University of Geosciences, Wuhan, China.
[3]Now at Planetary Science Institute, China University of Geosciences, Wuhan, China.
[4]Planetary Exploration Group, The Johns Hopkins University Applied Physics Laboratory, Laurel, Maryland, USA.
[5]Department of Terrestrial Magnetism, Carnegie Institution of Washington, Washington, D. C., USA.
[6]Lamont-Doherty Earth Observatory, Columbia University, Palisades, New York, USA.
[7]Planetary Science Institute, Tucson, Arizona, USA.
[8]Institute of Planetary Research, Deutsches Zentrum für Luft und Raumfahrt, Berlin, Germany.

Corresponding author: Z. Xiao, Lunar and Planetary Laboratory, University of Arizona, Tucson, AZ 85721, USA. (xiaobear@lpl.arizona.edu)

2169-9097/13/10.1002/jgre.20115

[4] The second low-reflectance spectral unit on Mercury has a reflectance ~30% lower than the global average [*Robinson et al*., 2008], displays a relatively blue spectral slope, and covers at least 15% of Mercury's surface. Termed "low-reflectance material" or LRM [*Robinson et al*., 2008; *Denevi et al*., 2009], the unit occupies broad areas with diffuse margins that are sometimes overlaid by smooth plains materials [*Denevi et al*., 2009]. LRM takes a variety of forms, including ejecta from large impact craters such as those inside the Caloris basin [*Robinson et al*., 2008]; as annular deposits surrounding impact basins such as Derain [*Denevi et al*., 2009], Rachmaninoff [*Prockter et al*., 2010], Tolstoj [*Robinson et al*., 2008], and Sobkou [*Denevi and Robinson*, 2008]; and as streaks of dark material excavated by impact craters, e.g., Mozart [*Robinson et al*., 2008]. Individual regions of LRM can be larger than 4×10^6 km^2 in area [*Denevi et al*., 2009]. Although most reported LRM is spatially associated with impact structures and therefore is interpreted to have been excavated from depth by impact cratering [e.g., *Denevi and Robinson*, 2008; *Robinson et al*., 2008; *Denevi et al*., 2009; *Ernst et al*., 2010], some areas of diffusely distributed LRM have no apparent relation to impact structures. In either situation, LRM may have originally been emplaced magmatically as intrusive or extrusive deposits but was subsequently modified and mixed through impact processes [*Denevi et al*., 2009]. The surface expression of LRM implies that there are vertical and horizontal variations in composition within the crust of Mercury, rather than only variations in the degree of modification by ion and micrometeoroid bombardment, i.e., space weathering [*Robinson et al*., 2008; *Denevi et al*., 2009].

[5] It has been suggested that the primary spectral difference between LRM and high-reflectance red plains (HRP), plains with higher reflectance and steeper or "redder" spectral slope than the average spectrum of Mercury [*Robinson et al*., 2008; *Denevi et al*., 2009], is the result of different abundances of opaque minerals [*Denevi and Robinson*, 2008; *Robinson et al*., 2008; *Denevi et al*., 2009; *Riner et al*., 2009; *Blewett et al*., 2009; *Lucey and Riner*, 2011]. Analysis of observations by MESSENGER's X-Ray Spectrometer (XRS) obtained since the spacecraft was inserted into orbit about Mercury in March 2011 indicates that the low-reflectance units generally contain somewhat more sulfur than the high-reflectance red plains [*Nittler et al*., 2011; *Weider et al*., 2012]. Whether this difference in sulfur abundance is a persistent distinction between LRM and HRP, however, or whether sulfur-bearing compounds constitute the opaque minerals that account for the different reflectances and colors of these two types of spectral unit is not clear.

[6] Images obtained by MESSENGER's Mercury Dual Imaging System (MDIS) [*Hawkins et al*., 2007] reveal that the bright crater-floor deposits first identified in Mariner 10 images [e.g., *Dzurisin*, 1977; *Robinson and Lucey*, 1997; *Robinson et al*., 2008], when viewed at high resolution from orbit, consist of irregularly shaped, rimless depressions often surrounded by high-reflectance material [*Blewett et al*., 2011, 2013]. Termed bright-haloed hollows, these features are interpreted to have formed from the loss of a crustal volatile component [*Blewett et al*., 2011], possibly one or more sulfides [*Vaughan et al*., 2012; *Blewett et al*., 2013; *Helbert et al*., 2013]. Hollows preferentially occur in LRM, indicating that the two units might be compositionally related and leading to several specific hypotheses for hollow formation [*Blewett et al*., 2011, 2013; *Vaughan et al*., 2012; *Helbert et al*., 2013].

[7] In this paper, we describe a subcategory of LRM on Mercury, here termed "dark spots." Dark spots consist of material with the lowest average reflectance yet observed on Mercury and display reflectance spectral slopes similar to those of other areas of LRM. When viewed at sufficiently high resolution, dark spots always host a central hollow. Dark spots may therefore provide important insight into both the composition of LRM and the formation and evolution of hollows.

[8] We have investigated dark spots with a combination of MDIS image products, including a global monochrome mosaic with a resolution of 250 m/pixel, high-resolution narrow-angle camera (NAC) targeted images (with resolution as good as 12 m/pixel), and eight-band color mosaics. In the following sections, we describe the morphology, size, occurrence, and spectral characteristics of dark spots, including the relationship between dark spots and hollows. We then discuss possible darkening agents for dark spots, estimate their ages, and finally propose a model for the origin of dark spots that links their formation with the initial stages of formation of hollows.

2. Characterization of Dark Spots

[9] Dark spots on Mercury are a type of low-reflectance material that can be found around hollows in thin deposits that have diffuse edges and are generally small in area. The characteristics of dark spots are well illustrated by several examples in Mercury's northern hemisphere (Figure 1). Dark spots have a reflectance that is lower than that of the surrounding terrain, including the Caloris exterior plains (classified as LBP) located to the southeast of the area shown in Figure 1a. The apparent albedos of dark spots are not uniform, however, even among dark spots in the same area. For example, at the 750 nm wavelength of the MDIS NAC images, the two dark spots in Figure 1e (indicated by the two red arrows) have reflectances of 0.03 and 0.02 (the method we follow for measuring calibrated reflectance values is described in section 2.3).

2.1. Morphology of Dark Spots

[10] Individual dark spots have smaller surface areas (usually less than ~100 km^2) than typical deposits of LBP and impact-excavated LRM. The dark spots in Figures 1c–1e, for example, have areas less than ~10 km^2. Dark spots tend to be isolated from each other, often appearing as small, discrete dark zones in regional-scale images (Figures 1a and 1b). The morphology and isolated occurrence of dark spots are more evident in high-resolution images (Figures 1c–1e). Moreover, dark spots have diffuse margins and appear to lack resolvable thicknesses. In some cases, the underlying terrain can be seen through the material that makes up the dark spot, especially toward the margins (e.g., Figure 1c).

[11] Each dark spot observed at sufficiently high resolution has an irregularly shaped, rimless depression in its center. Where the depressions are resolved, the floors of the depressions exhibit a higher reflectance than the surrounding dark spots (Figures 1c–1e). These characteristics indicate that the central depressions are not likely to be impact craters. Instead, they are morphologically similar to small hollows, features that are abundant across the surface of Mercury

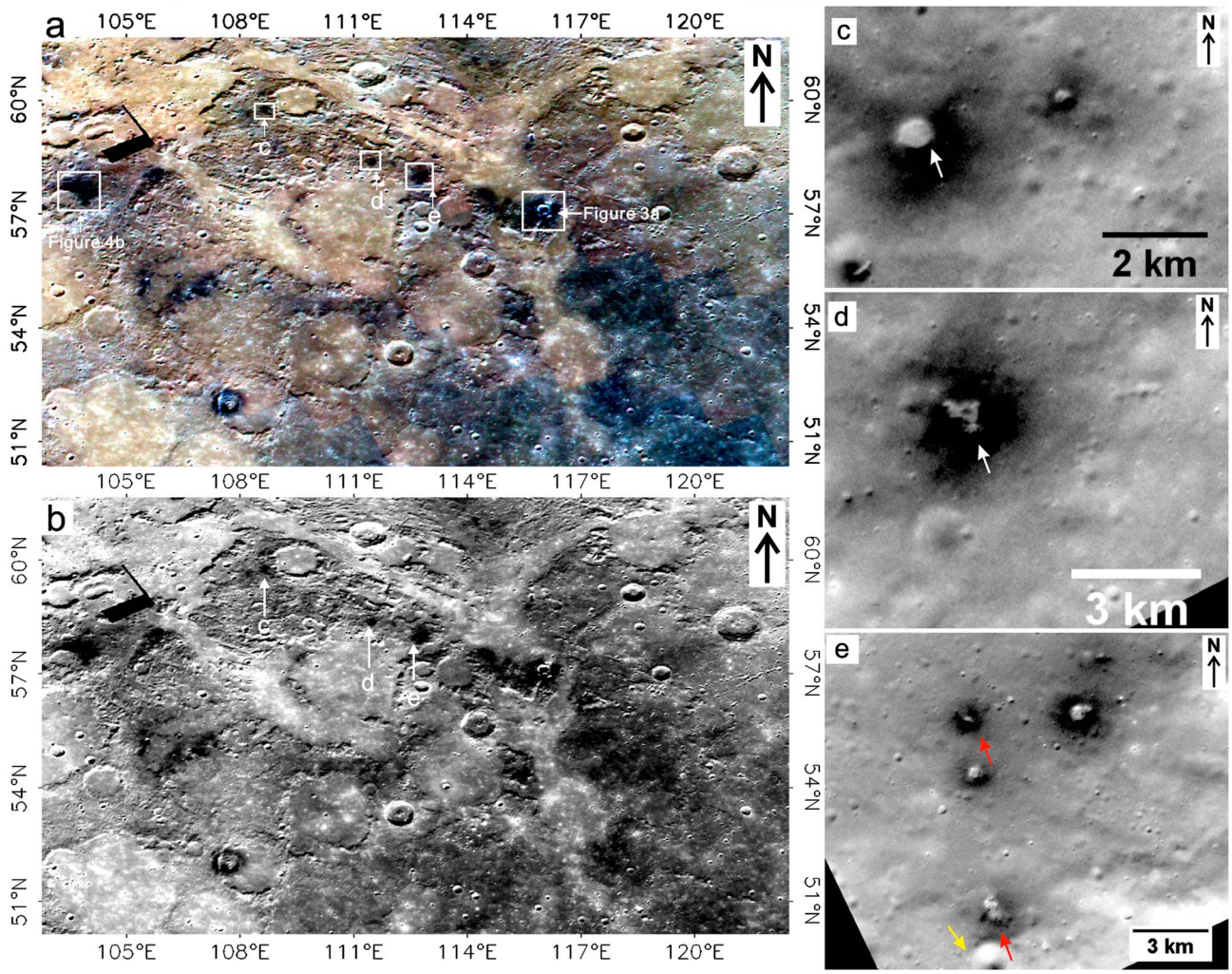

Figure 1. Examples of dark spots on Mercury. (a, b) MDIS color composite and monochrome mosaics (665 m/pixel), respectively, for an area in the northern hemisphere of Mercury. For the color mosaic, red (R), green (G), and blue (B) have been assigned to 1000, 750, and 430 nm wavelength, respectively. The images are portions of the MDIS global mosaics centered at 55.9°N, 112.6°E, and are in an equirectangular projection. White boxes denote the locations of Figures 1c–1e, 3a, and 4b. (c–e) Detailed morphology of several dark spots in this region, as shown in sinusoidal projection. The base image in Figure 1c is EN0234070626M (18 m/pixel), that for Figure 1d is from EN0233900778M (21 m/pixel), and that for Figure 1e is from EN0233900799M (20 m/pixel). The red arrows in Figure 1e show that dark spots and their central hollows are not proportional in size and that the two dark spots have different apparent albedos. The yellow arrow shows an impact crater that has not deposited dark ejecta.

[*Blewett et al*., 2011, 2013]. Further, the dark spot material is not likely to be LRM distributed by impact cratering, because no impact craters are visible in the centers of dark spot material and nearby larger fresh impact craters have no surrounding LRM (e.g., the yellow arrow in Figure 1e points to a crater ~1 km in diameter that has no LRM ejecta deposits). Moreover, as illustrated by the examples in Figure 1e (red arrows), the surface area of a dark spot is not proportional to the size of its central depression, i.e., large depressions can have a small dark spot, and vice versa.

2.2. Locations of Dark Spots

[12] From a combination of MDIS global color mosaics and targeted high-resolution monochrome images, we identified 34 dark spots on Mercury. Locations of individual features are shown in Figure 2 and listed in Table S1 in the supporting information. Like hollows on Mercury [*Blewett et al*., 2013], dark spots appear to be evenly distributed in longitude (Figure 2).

[13] We also identified another 48 areas of low-reflectance material that share some similarities with dark spots but for which the dark spot designation could not be assigned with confidence (Figure 2 and Table S1). Although these dark areas have diffuse margins and associated hollows and are spatially related to impact craters, it is not clear from available data whether such patches qualify as dark spots according to the usage of that term in this paper because they could also be small areas of impact-excavated LRM.

[14] Some examples of these possible dark spots are shown in Figure 3. Figure 3a shows LRM and hollows on the ejecta

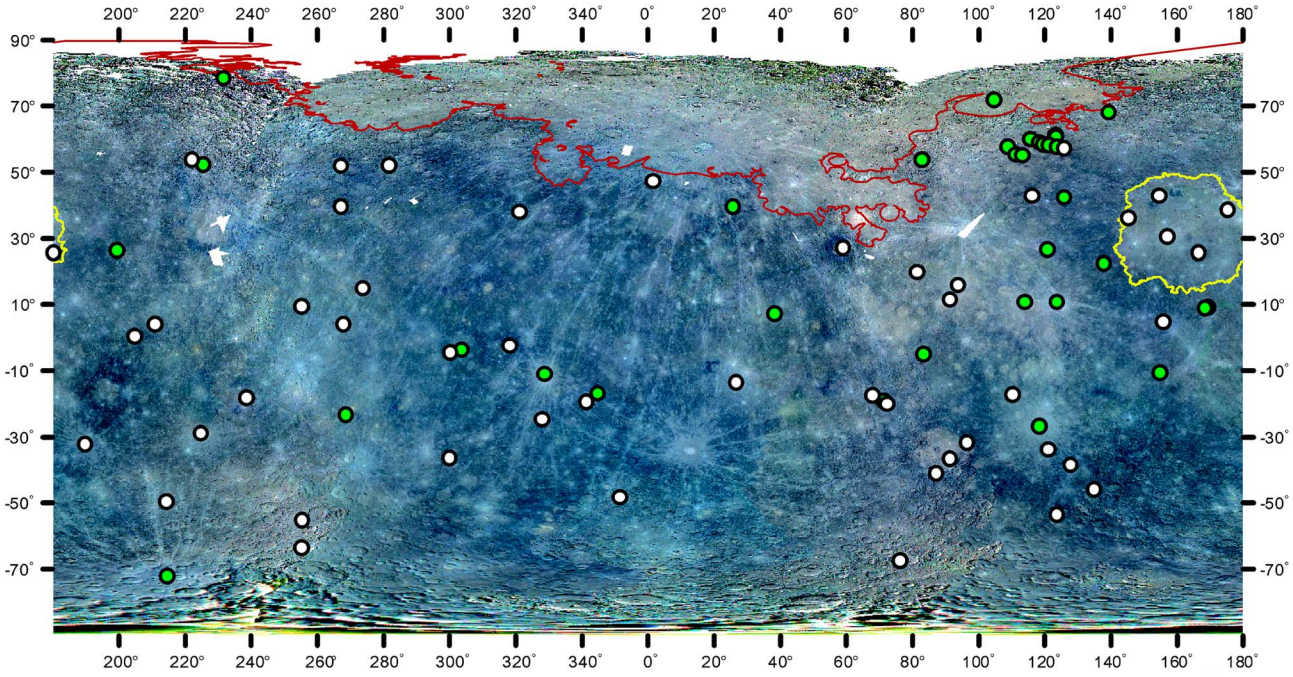

Figure 2. Locations of dark spots on Mercury. Green circles indicate confirmed dark spots, and white circles mark possible dark spots (Table S1). The locations of the dark spots are projected onto an MDIS global color mosaic of Mercury (665 m/pixel). The R, G, and B bands in this mosaic are at 1000, 750, and 430 nm wavelength, respectively. The map projection is equirectangular. Detailed information for this mosaic is available from the Planetary Data System (http://geo.pds.nasa.gov/missions/messenger/index.htm). The red line shows the boundary of the northern volcanic plains described by *Head et al*. [2011], and the yellow line marks the rim of the Caloris basin. Both the northern plains and the plains interior to Caloris are high-reflectance red plains. No dark spots have yet been identified on high-reflectance red plains material.

blanket and rim crest of a simple crater (9 km diameter; 57.1°N, 126.0°E). The LRM could represent either redistributed material excavated from depth [*Blewett et al*., 2013] or dark spots. In some situations, dark materials with different apparent albedos are found within a single impact crater, and the identification of the material as impact-excavated LRM or a dark spot cannot be readily made. For example, the Sholem Aleichem crater (196 km diameter; 51°N, 270°E) has dark ejecta deposits around its rim that might be impact-excavated LRM (yellow arrow in Figure 3b). Materials with a lower reflectance than the impact-excavated LRM are found on the western crater wall (white arrows), and bright haloed hollows are seen near the center of the low-reflectance area. Although the darker materials have the diffuse edges that are typical of dark spots, they might also be locally concentrated impact-excavated LRM. Figures 3c and 3d show another example of this albedo difference in the crater Tyagaraja (96.9 km diameter; 3.9°N, 221.3°E). Tyagaraja excavated subsurface LRM that is now visible on both the crater floor and the ejecta blanket. Extensive areas of bright-haloed hollows [*Blewett et al*., 2011] and reddish pyroclastic deposits [*Goudge et al*., 2012] are found on the crater floor (Figure 3c). At the foot of the southern central peak, material with a lower reflectance than the impact-excavated LRM is visible around some hollows (Figure 3d). Although this darker material features diffuse boundaries, it could be a dark spot or a small area of impact-excavated LRM.

[15] Confirmed dark spots occur on a variety of terrains on Mercury, including LBP, intercrater plains, heavily cratered terrain, and impact craters. Figure 4a shows a dark spot in the smooth plains of the Odin Formation, which form part of the Caloris exterior plains [*Fassett et al*., 2009]. Small depressions with a higher reflectance are seen in the central portions of the dark spot; an example is indicated by the white arrow in the lower left inset. Figure 4b shows a dark spot on intercrater plains (the location of this image is marked in Figure 1a). Numerous small depressions are visible in the center of the dark spot, and the larger ones have higher-reflectance areas in their interiors. Figure 4c shows a dark spot on heavily cratered terrain. The surrounding areas appear to have been superposed by relatively high-reflectance plains material (see the inset color image). This heavily cratered area may be dominated by impact-excavated LRM deposits, but the dark spot material exhibits a diffuse boundary and has a lower reflectance than the impact-excavated LRM as seen in the monochrome image, and hollows are visible inside the dark spot. Figure 4d shows dark spots and characteristically bright-haloed hollows on the floor of the Eminescu peak-ring basin (130 km diameter; 10.7°N, 114.3°E).

[16] We have not found dark spots on HRP material [*Denevi et al*., 2009, 2013]. Figure 2 shows that some dark spots are located in areas mapped as northern plains [*Head et al*., 2011] and Caloris interior plains [e.g., *Murchie et al*., 2008], both of which are HRP. These dark spots, however, are exclusively associated with impact craters that excavated subsurface LRM. For example, Figure 4e shows the only confirmed dark spot on the northern plains found to date

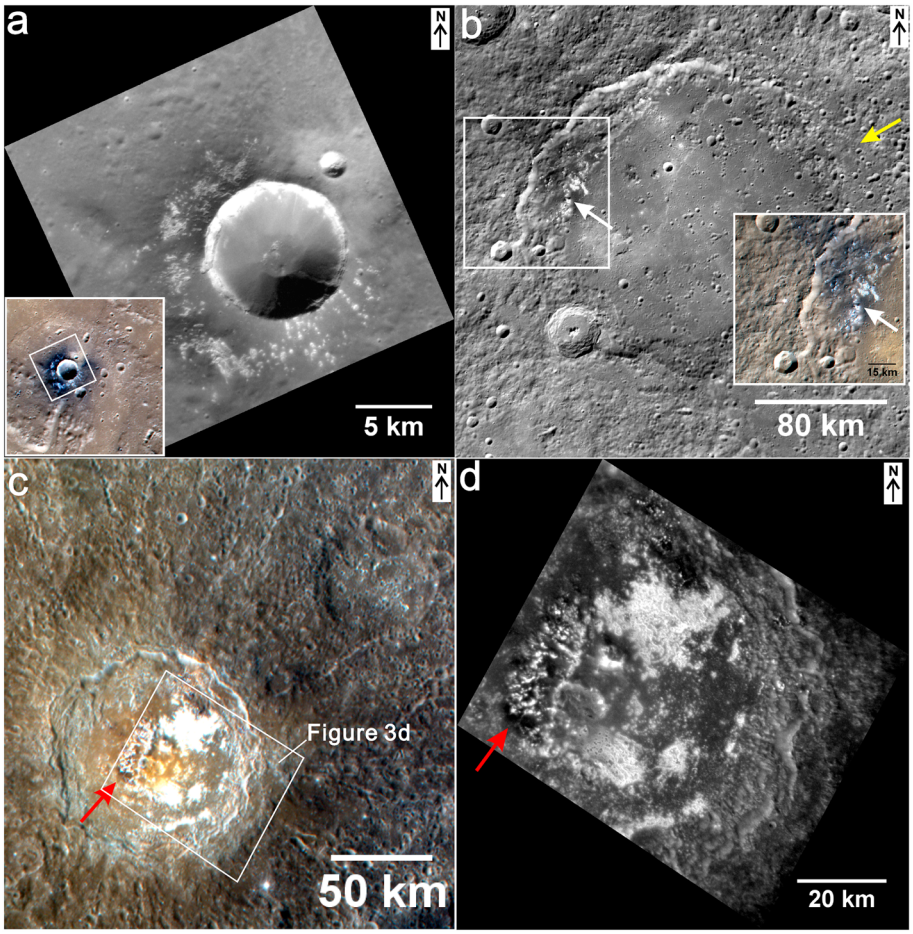

Figure 3. Examples of dark patches of LRM on Mercury that may be dark spots or may instead be impact-excavated LRM. All color images have R, G, and B assigned to 1000, 750, and 430 nm wavelength, respectively. (a) Dark materials and hollows occur on the ejecta blanket and rim crest of a simple crater (9 km diameter; 57.1°N, 126.0°E). The base image is EN0233815896M and is in sinusoidal projection (22 m/pixel). The location of the color image in the inset is marked in Figure 1a. (b) Sholem Aleichem crater has low-reflectance material around the crater rim that may be impact-excavated LRM (e.g., yellow arrow). A small patch of darker material occurs on the western crater wall (white arrow on main image and on color inset). This darker material could be impact-excavated LRM or a dark spot. The base mosaic is composed of MDIS images EW0211459892G, EW0211503353G, EW0211503457G, EW0211546686G, EW0211546814G, EW0211546918G, EW0211590147G, EW0211590275G, EW0211590379G, EW0211633734G, EW0211633839G, EW0211677193G, EW0211677297G, and EW0226668350G (234 m/pixel; sinusoidal projection). (c) Tyagaraja crater features excavated LRM on the ejecta deposits. Materials with a lower reflectance than the impact-excavated LRM may be seen at the foot of the southern central peak (red arrow). The color composite is from MDIS images EW0247654173G, EW0247654177F, and EW0247654181I (449 m/pixel; sinusoidal projection). (d) A monochrome image (EN0232711595M; 66 m/pixel, sinusoidal projection) shows the dark material on the southern floor of Tyagaraja (red arrow). The frame of this image is labeled as the white box shown in Figure 3c.

(yellow arrows). The dark spot is located on the floor of an impact crater that excavated subsurface LRM (red arrows in the color image).

2.3. Reflectance Spectra of Dark Spots

[17] Differences in composition and/or state of maturity of silicate surfaces affect their reflectance spectra [e.g., *Hapke*, 1977; *Fischer and Pieters*, 1994; *Lucey et al.*, 1998; *Warell and Valegård*, 2006; *Blewett et al.*, 2009]. To characterize the reflectance spectra of dark spots, we used MDIS wide-angle camera (WAC) images in eight filters from visible to near-infrared wavelengths (the central wavelengths are approximately 430, 480, 560, 630, 750, 830, 900, and 1000 nm [*Hawkins et al.*, 2007]). Since most dark spots are small in surface area, eight relatively large examples that provide better spectral statistics, together with four areas of LBP and eight examples of impact-excavated LRM, were selected for this study. The sampled areas of LBP are located in the Caloris exterior plains, and those of impact-excavated LRM are associated with several impact craters and basins, including Basho, Atget, Titian, Derain, Rachmaninoff, and Tolstoj. The locations and

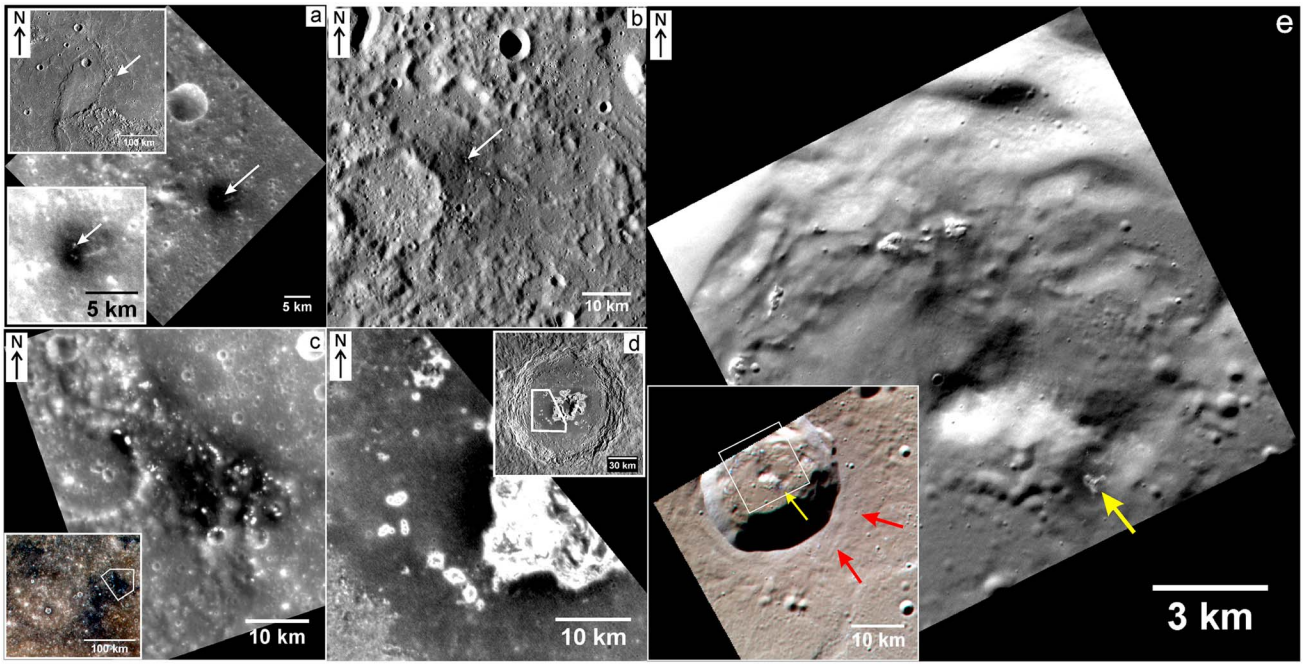

Figure 4. Dark spots on a variety of terrains on Mercury. All the color images have 1000, 750, and 430 nm wavelength displayed as R, G, and B, respectively. (a) A dark spot in the plains of Odin Planitia (arrows) centered at 26°N, 199.3°E. The upper left inset shows the general location of the dark spot from the global monochrome mosaic of Mercury. The main image shows the detailed morphology of the dark spot (MDIS EN0232669655M, 42 m/pixel; sinusoidal projection). The lower left inset is a portion of the main image with a different contrast stretch to show the small high-reflectance depressions in the center of the dark spot. (b) A dark spot (indicated by the white arrow) in intercrater plains in the northern hemisphere; the location of this image is shown in Figure 1a. The base image is EW0221152376G (60 m/pixel; sinusoidal projection). Small depressions are found in the center of the dark spot, and the larger depressions have a higher reflectance in their interiors. (c) A dark spot and its central bright-haloed hollows on heavily cratered terrain. The base image is EN0230920981M (53 m/pixel; sinusoidal projection). Its boundary is marked by the white outline in the inset color image (540 m/pixel; sinusoidal projection). Hollows are visible in the center of the dark spot. (d) Dark spots and bright-haloed hollows on the floor of the Eminescu peak-ring basin. The white box on the inset mosaic (EW0216155438G and EW0216155525G; 198 m/pixel; sinusoidal projection) shows the location of the high-resolution image (EN0219053353M; 62 m/pixel; sinusoidal projection). The hollows near the central peaks have surrounding dark spots, but some hollows on the flat crater floor do not have dark spots. (e) A dark spot on the northern volcanic plains is located in an impact crater that excavated subsurface LRM (red arrows). The outline in the inset shows the location of the main image. The yellow arrows show the dark spot and its central hollow. The main image is EN0249499289M (12 m/pixel; sinusoidal projection).

images used for analysis are listed in Table S2 in the supporting information.

[18] For each sampling site, a single MDIS image cube (eight bands) was used rather than an image mosaic in order to avoid difficulties in mosaicking caused by variations in scattered light [*Domingue et al*., 2011]. The MDIS images have incidence and emission angles less than 70° and phase angles less than 110°. They were photometrically corrected to reflectance at the standard bidirectional geometry of 30° phase angle, 30° incidence angle, and 0° emission angle [*Domingue et al*., 2011]. We used the U.S. Geological Survey's Integrated Software for Imagers and Spectrometers to calibrate the images and to derive the reflectance spectra. With improved image resolution and coverage of the MDIS orbital data compared with the MESSENGER flyby data, we were able to select the spectral sampling sites so as to avoid Sun-facing slopes, shadows, and crater rays. The spectral sampling areas were in all cases larger than one MDIS image pixel to decrease the uncertainties contributed by scattered light and image misregistration.

[19] Reflectance spectra of the sampled dark spots are shown in Figure 5a. Similar to previous findings for the spectral characteristics of Mercury [e.g., *McClintock et al*., 2008; *Denevi et al*., 2009], all the curves of the sampled dark spots have positive (i.e., red) slopes, and none shows evidence for a ferrous iron absorption band near 1000 nm wavelength. This last result is consistent with earlier findings that the surface of Mercury is generally low in ferrous iron (FeO) [e.g., *Vilas*, 1988; *Blewett et al*., 2002, 2009; *Strom and Sprague*, 2003; *Warell and Blewett*, 2004; *Robinson et al*., 2008; *Denevi et al*., 2009].

[20] The reflectances of the individual sampled dark spots differ from each other by as much as a factor of ~2

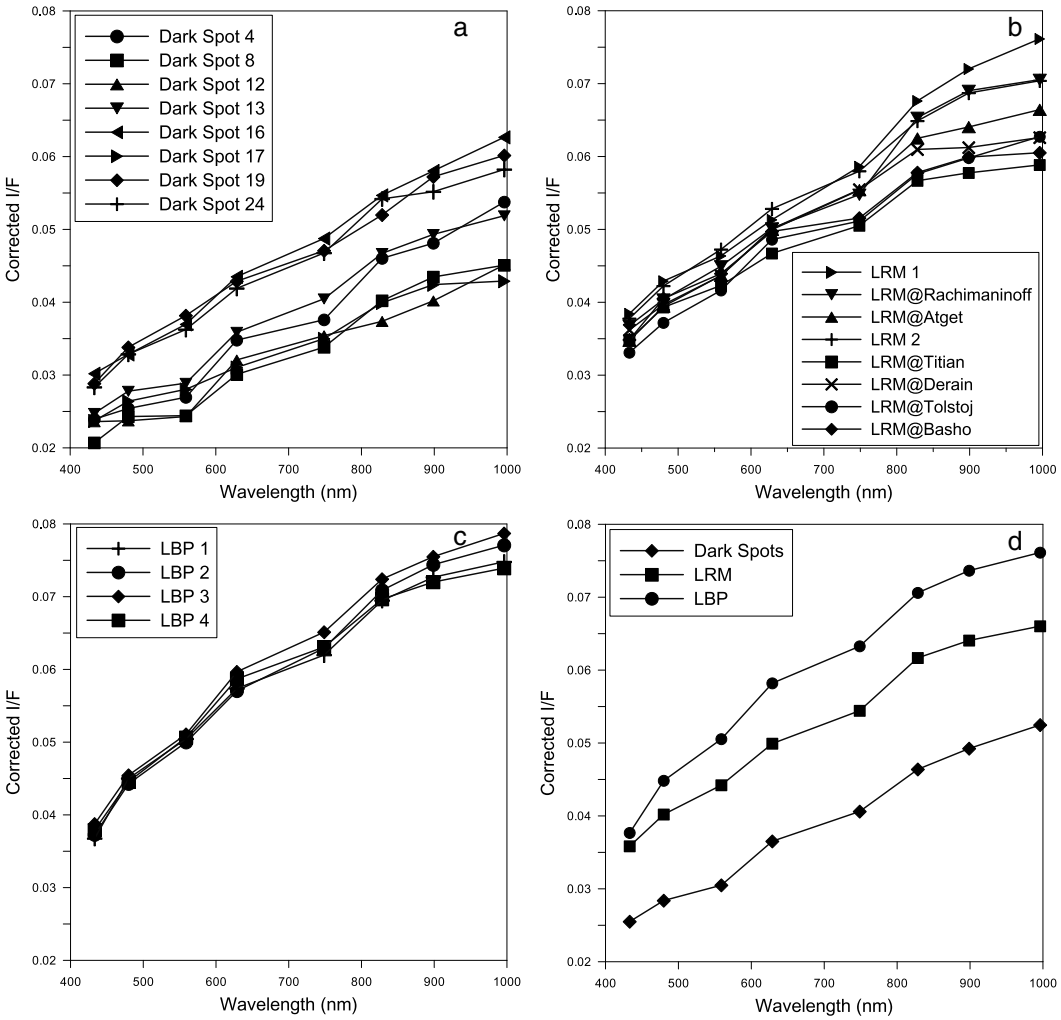

Figure 5. Photometrically corrected MDIS spectra for the sampled dark spots, impact-excavated LRM, and LBP on Mercury. The radiance factor, or reflectance [*Minnaert*, 1961], is the observed radiance *I* divided by the radiance *F* expected from a normally illuminated Lambertian surface [*Domingue et al*., 2011]. Table S2 in the supporting information provides information on the sampled sites. (a) Spectral comparison for eight representative dark spots. (b) Spectral comparison for eight representative areas of impact-excavated LRM. (c) Spectral comparison for four representative areas of LBP. (d) Averaged spectra of the dark spots compared with those of the LBP and impact-excavated LRM. The three types of color units substantially differ in albedo. The small variations in the spectral curves are within correction uncertainties.

(Figure 5a), a result consistent with the observation noted above that nearby dark spots can have different apparent albedos (Figure 1e). This difference might be caused by variations in the physical properties of the dark spot material (e.g., thickness and/or particle size), indicating that dark spot materials on emplacement may vary in reflectance. Alternatively, the different reflectances may be a result of different degrees of lateral or vertical mixing with material from underlying and adjacent terrain.

[21] In contrast, the spectra of the sampled LBP and impact-excavated LRM are more strongly clustered, as shown in Figures 5b and 5c. This clustering is consistent with the observation by *Denevi et al*. [2009] that LRM exhibits a small variation in spectral reflectance regardless of differences in age, deposit dimension, or mode of occurrence.

[22] Averaged spectra for the sampled dark spots, impact-excavated LRM, and LBP are compared in Figure 5d. Generally, the three types of dark units have a comparable spectral slope, and their major spectral difference is the absolute reflectance value, i.e., their albedo. The LBP exhibits reflectances ~20% above those of impact-excavated LRM and ~50% above those of dark spots.

[23] Comparison of Figures 5a and 5b shows that the dark spots with the highest reflectance values have spectral reflectance curves that overlap those for LRM (e.g., dark spot 16; see Table S1 in the supporting information). We cannot, therefore, distinguish dark spots as a group from LRM as earlier defined by *Robinson et al*. [2008] and *Denevi et al*. [2009] on the basis of spectral reflectance. Nonetheless, as may be seen in Figure 5d, the average reflectance of dark spot material is less than that of both LBP and impact-excavated LRM. Thus, on the basis of both the average spectra and the examples with the lowest reflectance, dark spots are the darkest material yet measured on Mercury. Further, on the basis of this distinction, it is

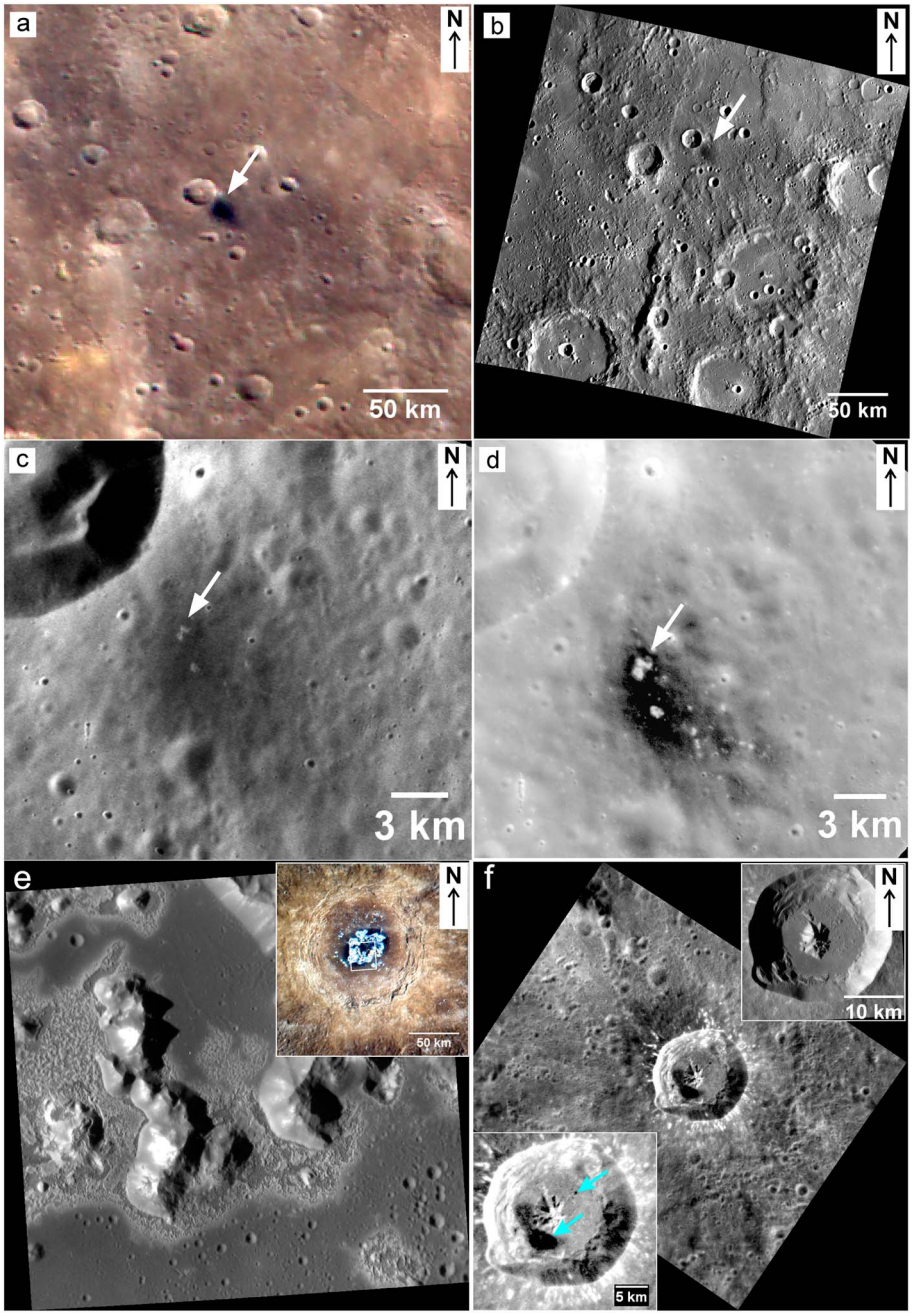

Figure 6. The importance of image resolution and incidence angle (i) in detecting and identifying hollows in the centers of dark spots. The white arrows in Figures 6a–6d point to the same dark spot centered at 39.4°N, 25.9°E. All the color images have 1000, 750, and 430 nm wavelength displayed as R, G, and B, respectively. All the panels are shown in sinusoidal projection. (a) MDIS color mosaic of the dark spot (665 m/pixel). (b) Monochrome image of the dark spot (EW0220030595G; 291 m/pixel; $i = 74°$). (c) A high-resolution image for the dark spot (EN0235512910M; 36 m/pixel; $i = 66°$). Two bright dots are seen in the center. (d) The dark spot is evident in EN0240207569M (26 m/pixel; stretched to show the hollows better), and the bright dots are identified as hollows in this high-resolution image. The incidence angle in this image is $i = 48°$. (e) Obvious dark spots on the southern floor of the Eminescu basin (color inset) are not clearly visible in the main image that was taken at an incidence angle of 67° (EN0221282722M, 25 m/pixel). (f) Dark spots are clearly shown on the eastern and western floors of Xiao Zhao crater. The main image is EN0218840436M (72 m/pixel) and was obtained with an incidence angle of 19°. The lower left inset is an enlargement for EN0218840436M showing the dark spots (blue arrows). The upper right inset is from MDIS EN0251488157M (34 m/pixel) and was obtained with an incidence angle of 70°. The dark spots are not readily visible in this inset.

possible that some or all of the dark spot material differs compositionally from impact-excavated LRM.

[24] It should be noted that the photometric calibration parameters for MDIS color images continue to be improved as more orbital data are collected and temporal variations are understood [*Keller et al*., 2013]. The spectral characteristics of the dark spot material, impact-excavated LRM, and LBP reported above should therefore be regarded as preliminary results that may change in response to further analysis. Moreover, the Mercury Atmospheric and Surface Composition Spectrometer (MASCS) instrument on MESSENGER [*McClintock et al*., 2008] has acquired globally distributed spectra of Mercury's surface at wavelengths of ~300–1400 nm with high spectral resolution. As targeted MASCS spectra for dark spot material continue to be returned by the MESSENGER mission, follow-on spectral studies of dark spots with MASCS data are clearly warranted.

3. Dark Spots and Hollows

3.1. Collocation of Dark Spots and Hollows

[25] Rimless depressions and bright-haloed hollows commonly occupy the centers of the observed dark spots (e.g., Figures 1 and 4). The depressions without bright halos also feature a higher reflectance in their interiors than the surrounding dark spots, although the higher reflectance can be identified only when the depressions are resolved in MDIS images of sufficiently high spatial resolution. When the depressions are small, it is difficult to determine if the apparent higher reflectance results from the bright Sun-facing walls or a higher albedo of the material within the depressions (Figure 4a). For depressions of greater sizes that are more easily resolved, the higher reflectance is seen to characterize material interior to the depressions. For example, the depression on the left in Figure 1c and that in Figure 1d (white arrows) both have a higher reflectance than the surrounding dark spots. The interiors of the depressions appear mostly flat, though larger examples sometimes exhibit small knobs, the tops of which may be remnants of the original surface, e.g., in the center of the depression shown in Figure 1d (white arrow). This morphological characteristic is also shared with hollows [*Blewett et al*., 2011, 2013]. For some larger depressions (greater than ~0.5 km^2 in area), bright halos are visible around the depressions, and these features resemble the typical bright-haloed hollows found elsewhere on the planet [*Blewett et al*., 2011, 2013]. For example, the hollows in Figure 4c cover an area of ~1.1 km^2 and are clearly haloed. Larger bright-haloed hollows may coalesce to resemble the "Swiss cheese terrain" on Mars [*Byrne and Ingersoll*, 2003], as in the case of hollows around the central peak of Eminescu (Figure 4d). The floors and halos of the hollows have a higher reflectance than both the surrounding dark spot material and background terrain [*Blewett et al*., 2011].

[26] Sufficient image resolution and low solar incidence angle (*i*, measured from the surface normal) are both critical to identifying whether the depressions in the centers of dark spots are hollows, just as such image characteristics are key to identifying the dark spots themselves. The pixel dimension required for such identification is ~30 m or better. Figure 6 illustrates the combined importance of high image resolution and low incidence angle. No hollows are seen in the center of the dark spot in the color mosaic shown in Figure 6a (665 m/pixel) or in the WAC monochrome image shown in Figure 6b (291 m/pixel; $i = 74°$). Two bright dots are visible in the center of the dark spot in the 36 m/pixel image shown in Figure 6c ($i = 66°$), but their morphology is not clear. In the 26 m/pixel image (Figure 6d, $i = 48°$), however, the irregularly shaped bright dots are resolved and appear to be small hollows, just like the examples shown in Figures 1c–1e. Figures 6e and 6f again show the importance of incidence angle. The dark spots on the southern crater floor of Eminescu are clearly visible in the color image shown in Figure 6e. However, the main image has a large incidence angle ($i = 67°$) so the dark spots are difficult to resolve, although the image has a better resolution (25 m/pixel) than that of Figure 4d (62 m/pixel). Similarly, in the lower left inset in Figure 6f, an enlargement of the main image that shows Xiao Zhao crater (24 diameter; 10°N, 124°E) at a resolution of 72 m/pixel and an incidence angle of 19°, two dark spots (blue arrows) are evident on the eastern and western crater floors. However, the dark spots are not visible in the upper right inset, which has a better resolution than the main image (34 m/pixel) but a greater incidence angle ($i = 70°$).

3.2. Hollows Without Surrounding Dark Spot Material

[27] Whereas all dark spots imaged with adequate resolution and incidence angle exhibit central hollows, not all hollows on Mercury are surrounded by dark spot material. Among the hollows mapped by *Blewett et al*. [2013], less than 30% have surrounding dark spot material. For example, on the floor of Eminescu, dark spot material is seen around only those hollows near the central peak complex, whereas smaller hollows in the flat part of the crater floor are not surrounded by dark spot material (Figure 4d). These observations yield two alternative hypotheses for the relationship between hollows and dark spots.

[28] The first hypothesis is that all hollows initially form with dark spots. Under this scenario, the material composing the dark spots may be comparatively unstable and have a shorter lifetime than the corresponding central hollow under surface conditions on Mercury, including the large diurnal variation in temperature (up to ~600°C) and the strong radiation environment [cf. *Lucey and Riner*, 2011]. Thin surface deposits of dark spot material may also rapidly lose their distinctive low reflectance as a result of vertical mixing with underlying material during impact gardening. If this first hypothesis is correct, then hollows currently surrounded by dark spots are younger than those lacking dark spots. This temporal behavior may also account for the observation that there are large variations in reflectance among individual dark spots (Figures 1e and 5a).

[29] Alternatively, some hollows may have formed without dark spots. Under this second hypothesis, there need be no age relationship between hollows with dark spots and those without them, or between darks spots with different reflectance.

3.3. Hollows and Dark Spots in Rayed Craters

[30] Support for the first hypothesis above would be provided if we could identify a newly formed hollow surrounded by a dark spot. Rayed craters are among the youngest landforms on airless silicate bodies such as the Moon and Mercury. The presence of collocated hollows and dark spots that postdate bright-rayed craters (the youngest crater population on Mercury) [*Xiao et al*., 2012] would

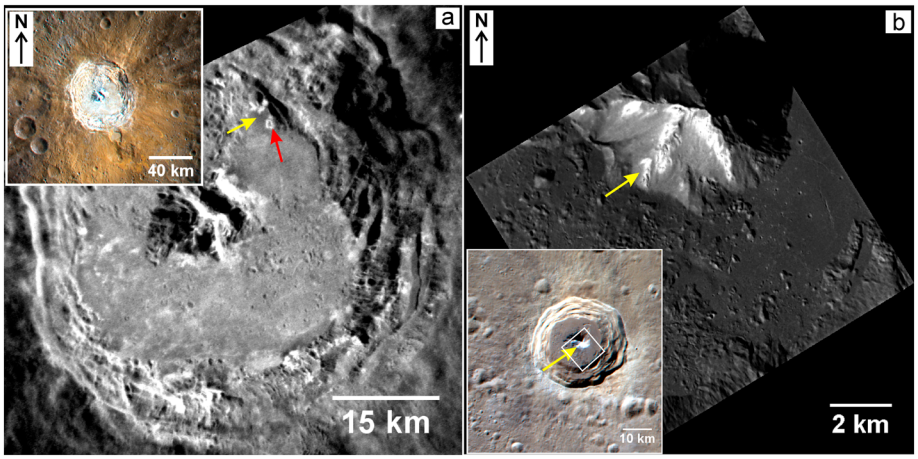

Figure 7. Hollows and dark spots in rayed craters on Mercury. (a) Kuiper crater has a pronounced ray system. Bright-haloed hollows (e.g., red arrow) occur on the crater floor, and dark spots are seen around the hollows (yellow arrow). The base image is EN0223659984M (75 m/pixel; sinusoidal projection). (b) A crater with fainter rays has bright-haloed hollows on its central peak (yellow arrows), but no dark spots are seen around these hollows, at least not on the sunlit slope. The base image is from EN0236617393M (20 m/pixel; sinusoidal projection). The insets in Figures 7a and 7b are MDIS color mosaics with R, G, and B assigned as 1000, 750, and 430 nm wavelength, respectively.

thus lend support to the possibility that all hollows initially form with dark spots, and those without dark spots represent a later evolutionary stage of hollows and are therefore generally older.

[31] To explore this issue, we consider Kuiper (62 km diameter; 11.3°S, 328.6°E), one of the most prominent rayed craters on Mercury (Figure 7a). No LRM is deposited on the continuous ejecta deposits, as seen in the color image (inset in Figure 7a). Small bright-haloed hollows ~1.3 km^2 in surface area are evident on the crater floor and along both the central peaks and the northern border of the crater wall (red arrow). Dark spots surround these hollows (yellow arrow). The same relationship between dark spots and collocated hollows is observed in other craters with distinctive rays, e.g., Han Kan (50 km diameter; 72°S, 214°E; MDIS EN0214987546M).

[32] Other rayed craters, however, have hollows that lack accompanying dark spots on their floors. Figure 7b shows such an example. This unnamed crater (~35 km diameter; 51°N, 94°E) has rays that are fainter than those of Kuiper. The rays are not easily visible in the color image (inset in Figure 7b), whereas the rays of Kuiper remain very prominent in color images such as Figure 7a. Bright-haloed hollows of ~2 km^2 area occur on the central peak, as indicated by the yellow arrow (Figure 7b), but dark spots are not seen around these hollows. Moreover, as noted above, some hollows on the floor of the morphologically fresh Eminescu peak-ring basin do not have a surrounding dark spot (Figure 4d). These hollows must also have formed in the Kuiperian [*Spudis and Guest*, 1988] because Eminescu is a Kuiperian-aged feature on the grounds that it possesses a system of faint rays [*Schon et al*., 2011].

[33] These examples suggest either that not all hollows initially form with dark spots or that dark spot material becomes indistinct on a time scale shorter than that of maturation of crater rays. Establishing the temporal order of rayed craters that host hollows with and without dark spots may help to distinguish between these two possibilities. For instance, the rays of the two parent craters in Figure 7 have a different apparent reflectance, indicating that the two craters might differ in age. If the hollows in Figure 7b and those on the floor of the faint-rayed Eminescu peak-ring basin initially developed with surrounding dark spots, such dark spots may have faded because of a somewhat longer exposure time than those in Kuiper (Figure 7a). However, it is also possible that the hollows shown in Figure 7b were initially not surrounded by dark spot material. Additional high-resolution imaging of dark spots and hollows associated with rayed craters displaying a range of apparent ages is needed to further evaluate the relationship between hollows and dark spot material.

4. Discussion

4.1. Ages of Dark Spots

[34] Dark spots represent one of the youngest endogenic surface units on Mercury. Dark spots that superpose craters with distinct rays, such as those on the crater floors of Kuiper (Figure 7a) and Xiao Zhao (blue arrows in Figure 6f), must be among the youngest, late-Kuiperian-aged features [*Spudis and Guest*, 1988]. As crater size-frequency distributions for all craters with distinct rays on Mercury give an average model age of ~270 Myr or less [*Xiao et al*., 2012], some dark spots may have formed subsequent to that time, and these enigmatic landforms may even be forming on Mercury today.

[35] In principle, we could bound the ages of dark spots and hollows more globally from the stratigraphic ages of their host terrain inferred from the areal density and morphology of related craters and from superposition relations [*Blewett et al*., 2013]. However, hollows and dark spots are relatively small surface features, and they are found on smooth plains, intercrater plains, and heavily cratered terrain (Figures 4a–4c) having crater retention ages of ~3.8 Gyr or more [cf. *Spudis and Guest*, 1988; *Strom et al*., 2008; *Denevi et al*., 2013].

Because dark spots and hollows can be substantially younger than their host terrains, the age constraints provided by stratigraphic relations are not of great value, except when the host area is a morphologically fresh crater.

4.2. Candidate Compositions for Dark Spot Material

[36] Both the confidently identified and possible dark spots occur only on surface units that have a lower reflectance than HRP material. Dark spots reported on HRP are exclusively associated with impact craters that have excavated subsurface LRM (e.g., Figure 4e). This distribution is consistent with that of hollows [*Blewett et al*., 2013]. *Robinson and Lucey* [1997] and *Robinson et al*. [2008] attributed the lower reflectance and bluer spectra of LRM than HRP to a higher content of opaque minerals in LRM, which they suggested might be Fe–Ti oxides. Results from MESSENGER's XRS indicate that the Fe and Ti abundances on Mercury are generally too low for ilmenite ($FeTiO_3$) to be present in sufficient concentrations to cause the low reflectance of Mercury overall, and the difference in spectral character between LRM and HRP in particular [*Nittler et al*., 2011].

[37] Sulfides could also lower Mercury's reflectance if present as opaque constituents [cf. *McClintock et al*., 2008]. XRS results show that at up to 4 wt % [*Nittler et al*., 2011], the sulfur content of Mercury's surface material is high but nonuniform [*Weider et al*., 2012]. For example, the northern plains [*Head et al*., 2011] and Caloris interior plains [*Strom et al*., 2008; *Head et al*., 2008; *Murchie et al*., 2008], both classified spectrally as HRP, have somewhat lower sulfur contents than surrounding terrains that are lower in reflectance [*Weider et al*., 2012]. Differences in sulfur content may thus contribute to differences in reflectance across the surface of Mercury [*Nittler et al*., 2011; *Weider et al*., 2012]. Because dark spots on Mercury occur only on material lower in reflectance than HRP, sulfides or other sulfur-bearing compounds could serve as darkening agents for dark spot material.

[38] Another argument that dark spot material might be richer in sulfur or sulfides than the average composition of Mercury's surface material is its spatial association with hollows. *Blewett et al*. [2013] and *Vaughan et al*. [2012] suggested that hollow-forming material is likely to be comparatively rich in sulfur or sulfides. As noted above, dark spots imaged at sufficiently high resolution always have hollows in their central regions. This observation indicates that dark spot material might have also been relatively rich in a volatile-bearing material at the time of formation, contributing to the diffuse boundaries of the deposits. Such material might be a sulfur-containing darkening agent similar, but not necessarily identical, to that of impact-excavated LRM. This possibility is supported by recent laboratory experiments indicating that some sulfides can be thermally decomposed at temperatures of less than 500°C, i.e., comparable to Mercury's maximum dayside temperatures [*Helbert et al*., 2013]. The idea that sulfides constitute the darkening phase in dark spot material could therefore also account for the observation that dark spots have different reflectance values (Figure 5a).

[39] XRS measurements show a correlation between sulfur and calcium abundances on Mercury's surface [*Nittler et al*., 2011; *Weider et al*., 2012], hinting that CaS may be an important surface mineral. Although magnesium and calcium sulfides have both been postulated as candidate hollow-forming materials on Mercury [*Vaughan et al*., 2012], *Helbert et al*. [2013] found that these sulfides were not particularly dark in room temperature measurements of reflectance at visible to near-infrared wavelengths. Our observation that dark spots are the darkest material yet observed on Mercury may thus point to another darkening component in dark spot material. Alternatively, Mercury's surface environmental conditions (e.g., high temperatures and strong radiation) may produce lower reflectance values for magnesium and calcium sulfides than those measured at room temperatures [*Helbert et al*., 2013]. Our current understanding of the composition of Mercury's crustal material is not sufficient to reveal why dark spots and hollows have markedly different albedos if they are both richer in sulfides than the average surface composition on Mercury, or how the darkening agents in dark spots and impact-excavated LRM might differ. Additional spectral comparisons of dark spots, hollows, and impact-excavated LRM, future inclusion of MASCS data, and ongoing laboratory spectral studies for sulfides under a simulated Mercury surface environment [*Helbert et al*., 2013] will be helpful to gain more insight into these issues.

4.3. A Possible Formation Mechanism and Evolutionary Sequence for Dark Spots

[40] Three genetic mechanisms for dark spots can be ruled out on the basis of the observations discussed above. First, dark spots do not directly form from impact cratering because they are not always associated with impact craters (e.g., Figures 1 and 4). Second, dark spots cannot represent localized outcrops of LBP because of their different sizes and contrast in reflectance (Figures 1a, 4a, and 5d). Third, explosive volcanism is not an obvious mechanism for the formation of dark spots because the small, irregularly shaped, shallow, and rimless hollows at the centers of dark spots have floors and sometimes bright haloes that differ in reflectance and spectral properties from the surrounding dark material [*Blewett et al*., 2013]. These characteristics differ from those of reddish and diffusely distributed material around rimless depressions on Mercury, which are interpreted as sites of explosive volcanic eruptions [*Kerber et al*., 2009, 2011; *Goudge et al*., 2012].

[41] Because all dark spots imaged at sufficiently high resolution have central hollows, we postulate that the two types of features are causally related. As with bright-haloed hollows, dark spots can be regarded as low-reflectance halos of their central hollows. However, there are important differences. Bright halos are located proximal to the rims of their associated hollows [*Blewett et al*., 2013] and somewhat overlap with the lightly pitted area around some hollows (Figure 6c) [*Vaughan et al*., 2012]. Dark spots, in contrast, extend several kilometers from their central hollows (Figures 1 and 4). The different radial extents of dark spots and bright halos indicate that the two types of features may have different modes of emplacement. Whatever the volatile component in the dark spot material is, one or more processes must distribute this material on the surface and produce the characteristic diffuse boundaries of the deposits.

[42] Dark spots on Mercury are morphologically similar to the dark spots at the south polar region of Mars (although not in scale or detailed structure), as both are diffusely distributed and surficial dark material located near central depressions.

Table 1. Radial Extent of Several Dark Spots on Mercury and Inferred Outgassing Velocities of Dark Spot Material

Dark Spot	Surface Area[a] (km^2)	Average Radial Extent[b] (km)	Outgassing Velocity[c] (m/s)
Figure 1c (left)	8.5	1.7	79
Figure 1d	10.2	1.8	82
Figure 1e (upper right)	8.6	1.7	79
Figure 4a	52.4	4.1	123
Figure 4b	72.0	4.8	133

[a]The surface area s is approximate because the dark spots have diffuse margins.

[b]The average radial extent r is calculated from the surface area s. Dark spots are taken to be circular, i.e., $s=\pi r^2$, so $r=s^{0.5}/\pi$.

[c]The ballistic trajectory on an airless body is given by $r=(v^2/g)\sin(2\theta)$, where r is range, v is the outgassing velocity, g is the surface gravitational acceleration (3.7 m/s^2 on Mercury), and θ is the trajectory angle measured from the zenith, here taken to be 45°. An angle larger or smaller than 45° requires a greater outgassing velocity for a given trajectory distance.

The Martian dark spots are interpreted to form by outgassing of a mixture of CO_2 and dust [e.g., *Kieffer et al*., 2006]. Dark spots on Mercury also somewhat resemble the reddish pyroclastic deposits on Mercury in planform though not in scale or color, as both types of feature are surficial deposits with diffuse edges [*Kerber et al*., 2009, 2011; *Goudge et al*., 2012].

[43] Because each dark spot on Mercury observed at sufficiently high resolution has a central hollow (large or small, bright or not), the dark spot material may have originated from the location of the hollow. Given the association of hollows with loss of volatile-rich material [*Vaughan et al*., 2012; *Blewett et al*., 2013; *Helbert et al*., 2013], dark spot material may have been dispersed by the release of a volatile compound, providing the initial velocity for ballistic emplacement of material up to several kilometers from the central hollow. Therefore, we suggest that dark spot material might be emplaced in a manner similar to material deposited by an outgassing event, as part of a contemporaneous process that resulted in the formation of an embryonic hollow.

[44] We estimated the approximate release velocity required for the distribution of dark spot material by measuring the average radial extent, derived from their surface area, of several dark spots. The expression for ballistic trajectories on airless bodies was employed to calculate the velocity at an assumed release angle (measured from the zenith) of 45°. The results of this analysis are shown in Table 1. Exit velocities of up to ~100 m/s were calculated, attesting to an energetic formation process. For release angles other than 45°, the ejection velocities would be even higher. The large outgassing velocities require the subsurface accumulation of dark-spot-forming material having a high content of volatiles and a large pressure that both depend on the depth and size of the reservoir. *Kerber et al*. [2009] employed the same calculation method to estimate the eruption velocities for explosive volcanic eruptions on Mercury that formed pyroclastic deposits. Because pyroclastic deposits generally have a larger radial extent than dark spots, such calculations indicate that explosive volcanic eruptions usually have larger ejection velocities than those indicated for dark spot formation. If dark spots were formed by such volatile-release events, development of a subsurface void in the crustal location from which the dark spot material originated could have led to the formation of a surficial depression by collapse of the overlying material, thus providing a mechanism for the development of a central hollow.

[45] This scenario does not imply, however, that continued hollow growth remained such an energetic process. Indeed, the horizontal growth rate of hollows is relatively slow: *Blewett et al*. [2011] estimated a lower limit for the average growth rate for the hollows in the Raditladi basin of ~0.14 μm/yr. Therefore, our calculations are suggestive only of the rapid formation of an initial (embryonic) hollow without a bright halo, followed by subsequent and sustained loss of hollow-forming materials at a markedly lower rate. Furthermore, as noted above, some hollows may form without dark spots, so the scenario described here may apply only to those hollows that are central to dark spots.

[46] Several unresolved issues with such an outgassing scenario for the origin of dark spots remain. The process by which dark spot material accumulates in the subsurface prior to an outgassing event is unknown. The loss of hollow-forming material has been postulated to be driven by some combination of solar heating and contact heating from impact melt or subsurface magmatic intrusions [*Blewett et al*., 2013; *Helbert et al*., 2013]. Similar processes may have acted to concentrate the dark-spot-forming material at depth, through the development of a subsurface reservoir comparatively rich in volatiles. Moreover, the reason for the initiation of formation of a dark spot is not known. A possible mechanism is overpressurization of accumulated dark spot material in the subsurface reservoir relative to lithostatic pressure (similar to the formation mechanism for polar dark spots on Mars) [*Kieffer et al*., 2006], leading to an outgassing event. Alternatively, a nearby impact cratering or seismic event may release subsurface dark spot material along proximal fractures.

[47] With this possible formation mechanism for dark spots, and on the basis of the observed relationship between dark spots and hollows and notwithstanding the uncertainties, we propose a three-stage evolutionary sequence for dark spots and their central hollows, with each stage represented by example areas observed on Mercury's surface (Figure 8).

[48] 1. After the subsurface accumulation of dark-spot-forming material, a dark spot forms energetically by outgassing from a small central hollow when a release of volatiles occurs (white arrow in Figure 8a). The floor of the hollow is bright when seen in high-resolution images. The newly formed dark spot begins to fade on exposure to Mercury's surface environment.

[49] 2. The embryonic hollow continues to grow, and bright halos develop around the hollow (white arrow in Figure 8b). This process is probably much slower than stage 1. The dark spot material remains visible but becomes progressively more faint, probably because of removal or modification by surface processes or through lateral or vertical mixing by impact gardening.

[50] 3. Finally, the dark spot fades entirely on a time scale comparable to or less than that for optical maturation of crater rays, whereas its central hollow continues to grow (white arrow in Figure 8c). The growth process of a hollow might follow that proposed by *Vaughan et al*. [2012], *Blewett et al*. [2013], or *Helbert et al*. [2013], but in any case, the central hollow has a longer lifetime than its surrounding dark spot.

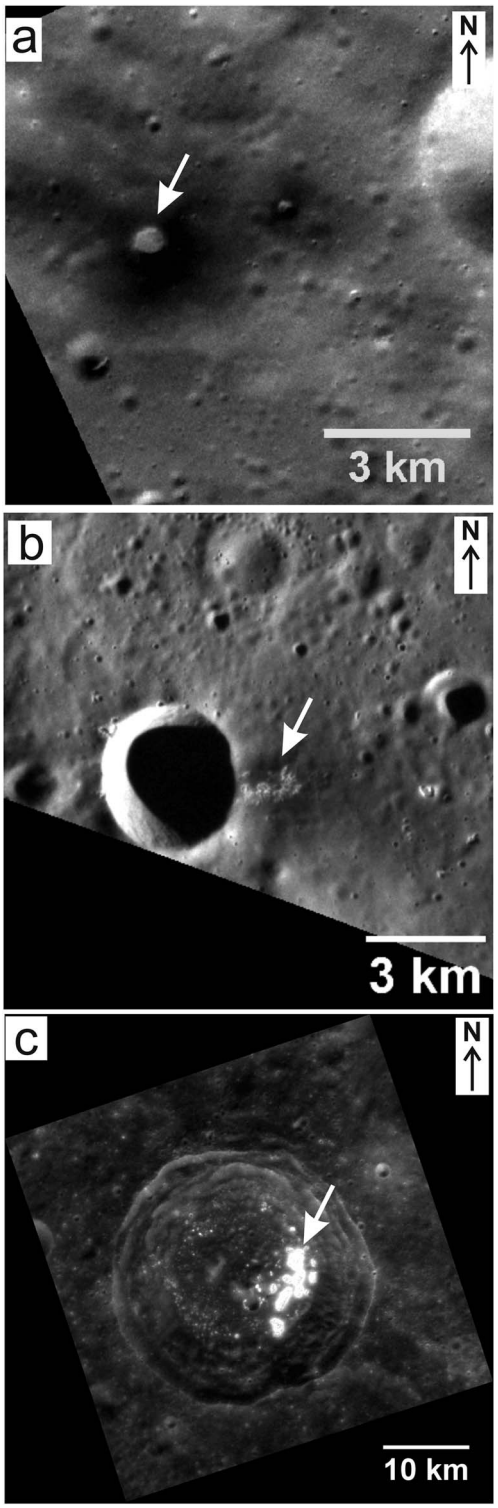

Figure 8. (a–c) A possible evolutionary sequence for dark spots and their central hollows. The base images in Figures 8a–8c are EN0234070626M (18 m/pixel), EN0231437939M (16 m/pixel), and EN0225905701M (44 m/pixel), respectively. The arrows in each image point to the dark spots and/or hollows. All the images are shown in sinusoidal projection. See section 4.3 for a detailed discussion.

5. Conclusions

[51] We have identified isolated hollow-related dark material on Mercury that we term dark spots. Dark spot material is a distinctive category of low-reflectance material on Mercury [*Robinson et al*., 2008; *Denevi et al*., 2009]. Dark spots are seen in small and thin surface deposits that are widely distributed with longitude. Such spots contain the darkest material yet identified on Mercury.

[52] Our analysis indicates the following characteristics of dark spots.

[53] 1. Dark spots are found on intercrater plains, low-reflectance blue plains, heavily cratered terrain, and impact craters. Dark spots have not yet been found on high-reflectance plains material, but some impact craters that penetrated high-reflectance plains and excavated subsurface low-reflectance material host dark spots.

[54] 2. Dark spot material is neither subsurface material directly redistributed by impact cratering nor pyroclastic deposits emplaced by the more common forms of explosive volcanism documented for Mercury. Dark spots may be enriched in sulfides or other sulfur-bearing compounds.

[55] 3. All dark spots have hollows in their central regions when viewed at sufficiently high resolution (~30 m/pixel or better). However, most hollows on Mercury do not have surrounding dark spots. Hollows may all form with dark spots that fade on a time scale shorter than the typical hollow lifetime, or some hollows may form in a manner that does not produce a dark spot. No proportional size relationship between dark spots and their central hollows has been established.

[56] 4. A possible formation mechanism for dark spots is by ballistic emplacement during release of volatile-rich material from an embryonic hollow. Under this scenario, a depression forms contemporaneously with the sudden release of dark material. From the radial extents of dark spots, exit velocities of dark spot material can exceed 100 m/s. Bright halos develop around the steadily growing hollow over a much longer time scale than that of dark spot formation.

[57] 5. Dark spots are one of the youngest endogenic terrains on Mercury. Once exposed to the surface environment of Mercury, the contrast between dark spots and their surroundings likely lessens with time in response to modification or removal of the darkening phases or regolith gardening until the dark spots fade from recognition.

[58] The role of outgassing in the formation and evolution of dark spots warrants further elaboration and quantification. Moreover, knowledge of the composition of dark spot material and its relationship to hollow-forming material would benefit from additional high-resolution elemental remote sensing and spectral measurements in areas containing dark spots and hollows.

[59] **Acknowledgments.** We thank Brett Denevi, Carolyn Ernst, and an anonymous reviewer for constructive comments that substantially improved this paper. Kris Becker kindly helped in the processing of MDIS images. The MESSENGER project is supported by the NASA Discovery Program under contract NAS5-97271 to The Johns Hopkins University Applied Physics Laboratory and contract NASW-00002 to the Carnegie Institution of Washington. D.T.B. is supported by a NASA MESSENGER Participating Scientist Program grant (NNX08AN29G).

References

Blewett, D. T., B. R. Hawke, and P. G. Lucey (2002), Lunar pure anorthosite as a spectral analog for Mercury, *Meteorit. Planet. Sci.*, *37*, 1245–1254.

Blewett, D. T., M. S. Robinson, B. W. Denevi, J. J. Gillis-Davis, J. W. Head, S. C. Solomon, G. M. Holsclaw, and W. E. McClintock (2009), Multispectral images of Mercury from the first MESSENGER flyby: Analysis of global and regional color trends, *Earth Planet. Sci. Lett.*, *285*, 272–282.

Blewett, D. T., et al. (2011), Hollows on Mercury: MESSENGER evidence for geologically recent volatile-related activity, *Science*, *333*, 1856–1859, doi:10.1126/science.1211681.

Blewett, D. T., et al. (2013), Mercury's hollows: Constraints on formation and composition from analysis of geological setting and spectral reflectance, *J. Geophys. Res. Planets*, *118*, 1013–1032, doi:10.1029/2012JE004174.

Byrne, S., and A. P. Ingersoll (2003), A sublimation model for Martian south polar ice features, *Science*, *299*, 1051–1053.

Denevi, B. W., and M. S. Robinson (2008), Mercury's albedo from Mariner 10: Evidence for the presence of ferrous iron, *Icarus*, *197*, 239–246.

Denevi, B. W., et al. (2009), The evolution of Mercury's crust: A global perspective from MESSENGER, *Science*, *324*, 613–618.

Denevi, B. W., et al. (2013), The distribution and origin of smooth plains on Mercury, *J. Geophys. Res. Planets*, *118*, 891–907, doi:10.1002/jgre.20075.

Domingue, D. L., S. L. Murchie, B. W. Denevi, N. L. Chabot, D. T. Blewett, N. R. Laslo, R. M. Vaughan, H. K. Kang, and M. K. Shepard (2011), Photometric correction of Mercury's global color mosaic, *Planet. Space Sci.*, *59*, 1873–1887.

Dzurisin, D. (1977), Mercurian bright patches: Evidence for physio-chemical alteration of surface material?, *Geophys. Res. Lett.*, *4*, 383–386, doi:10.1029/GL004i010p00383.

Ernst, C. M., S. L. Murchie, O. S. Barnouin, M. S. Robinson, B. W. Denevi, D. T. Blewett, J. W. Head, N. R. Izenberg, S. C. Solomon, and J. H. Roberts (2010), Exposure of spectrally distinct material by impact craters on Mercury: Implications for global stratigraphy, *Icarus*, *209*, 210–223, doi:10.1016/j.icarus.2010.05.022.

Fassett, C. I., J. W. Head, D. T. Blewett, C. R. Chapman, J. L. Dickson, S. L. Murchie, S. C. Solomon, and T. R. Watters (2009), Caloris impact basin: Exterior geomorphology, stratigraphy, morphometry, radial sculpture, and smooth plains deposits, *Earth Planet. Sci. Lett.*, *285*, 297–308.

Fischer, E. M., and C. M. Pieters (1994), Remote determination of exposure degree and iron concentration of lunar soil using VIS-NIR spectroscopic methods, *Icarus*, *111*, 475–488.

Goudge, T. A., et al. (2012), Global inventory and characterization of pyroclastic deposits on Mercury: New insights into pyroclastic activity from MESSENGER orbital data, *Lunar Planet. Sci.*, *43*, abstract 1325.

Hapke, B. (1977), Interpretations of optical observations of Mercury and the Moon, *Phys. Earth Planet. Inter.*, *15*, 264–274.

Hawkins, S. E., II, et al. (2007), The Mercury Dual Imaging System on the MESSENGER spacecraft, *Space Sci. Rev.*, *131*, 247–338, doi:10.1007/s11214-007-9266-3.

Head, J. W., et al. (2008), Volcanism on Mercury: Evidence from the first MESSENGER flyby, *Science*, *321*, 69–72, doi:10.1126/science.1159256.

Head, J. W., et al. (2011), Flood volcanism in the northern high latitudes of Mercury revealed by MESSENGER, *Science*, *333*, 1853–1856.

Helbert, J., A. Maturilli, and M. D'Amore (2013), Visible and near-infrared reflectance spectra of thermally processed synthetic sulfides as a potential analog for the hollow forming materials on Mercury, *Earth Planet. Sci. Lett.*, *369–370*, 233–238.

Keller, M. R., et al. (2013), Time-dependent calibration of MESSENGER's wide-angle camera following a contamination event, *Lunar Planet. Sci.*, *44*, abstract 2489.

Kerber, L., J. W. Head, S. C. Solomon, S. L. Murchie, D. T. Blewett, and L. Wilson (2009), Explosive volcanic eruptions on Mercury: Eruption conditions, magma volatile content, and implications for interior volatile abundances, *Earth Planet. Sci. Lett.*, *285*, 263–271.

Kerber, L., J. W. Head, D. T. Blewett, S. C. Solomon, L. Wilson, S. L. Murchie, M. S. Robinson, B. W. Denevi, and D. L. Domingue (2011), The global distribution of pyroclastic deposits on Mercury: The view from MESSENGER flybys 1–3, *Planet. Space Sci.*, *59*, 1895–1909.

Kieffer, H. H., P. R. Christensen, and T. N. Titus (2006), CO_2 jets formed by sublimation beneath translucent slab ice in Mars' seasonal south polar ice cap, *Nature*, *442*, 793–796, doi:10.1038/nature04945.

Lucey, P. G., and M. A. Riner (2011), The optical effects of small iron particles that darken but do not redden: Evidence of intense space weathering on Mercury, *Icarus*, *212*, 451–462.

Lucey, P. G., D. T. Blewett, and B. R. Hawke (1998), Mapping the FeO and TiO_2 content of the lunar surface with multispectral imaging, *J. Geophys. Res.*, *103*, 3679–3699.

McClintock, W. E., et al. (2008), Spectroscopic observations of Mercury's surface reflectance during MESSENGER's first Mercury flyby, *Science*, *321*, 62–65.

Minnaert, M. (1961), Photometry of the Moon, in *Planets and Satellites*, edited by G. P. Kuiper and B. M. Middlehurst, pp. 213–248, Univ. of Chicago Press, Chicago, Ill.

Murchie, S. L., et al. (2008), Geology of the Caloris basin, Mercury: A view from MESSENGER, *Science*, *321*, 73–76.

Murray, B. C., et al. (1974), Mercury's surface: Preliminary description and interpretation from Mariner 10 pictures, *Science*, *185*, 73–76.

Nittler, L. R., et al. (2011), The major-element composition of Mercury's surface from MESSENGER X-ray spectrometry, *Science*, *333*, 1847–1850, doi:10.1126/science.1211567.

Prockter, L. M., et al. (2010), Evidence for young volcanism on Mercury from the third MESSENGER flyby, *Science*, *329*, 668–671.

Riner, M. A., P. G. Lucey, S. J. Desch, and F. M. McCubbin (2009), Nature of opaque components on Mercury: Insights into a Mercurian magma ocean, *Geophys. Res. Lett.*, *36*, L02201, doi:10.1029/2008GL036128.

Robinson, M. S., and P. G. Lucey (1997), Recalibrated Mariner 10 color mosaics: Implications for Mercurian volcanism, *Science*, *275*, 197–200.

Robinson, M. S., et al. (2008), Reflectance and color variations on Mercury: Regolith processes and compositional heterogeneity, *Science*, *321*, 66–69.

Schon, S. C., J. W. Head, D. M. H. Baker, C. M. Ernst, L. M. Prockter, S. L. Murchie, and S. C. Solomon (2011), Eminescu impact structure: Insight into the transition from complex crater to peak-ring basin on Mercury, *Planet. Space Sci.*, *59*, 1949–1959.

Solomon, S. C., et al. (2001), The MESSENGER mission to Mercury: Scientific objectives and implementation, *Planet. Space Sci.*, *49*, 1445–1465.

Spudis, P. D., and J. E. Guest (1988), Stratigraphy and geologic history of Mercury, in *Mercury*, edited by F. Vilas, C. R. Chapman, and M. S. Matthews, pp. 118–164, Univ. of Arizona Press, Tucson, Ariz.

Strom, R. G., and A. L. Sprague (2003), *Exploring Mercury*, Springer-Praxis Books in Astronomy and Space Sciences, Springer, London, 216 pp.

Strom, R. G., C. R. Chapman, W. J. Merline, S. C. Solomon, and J. W. Head (2008), Mercury cratering record viewed from MESSENGER's first flyby, *Science*, *321*, 79–81, doi:10.1126/science.1159317.

Vaughan, W. M., J. Helbert, D. T. Blewett, J. W. Head, S. L. Murchie, K. Gwinner, T. J. McCoy, and S. C. Solomon (2012), Hollow-forming layers in impact craters on Mercury: Massive sulfide or chloride deposits formed by impact melt differentiation?, *Lunar Planet. Sci.*, *43*, abstract 1187.

Veverka, J., P. Helfenstein, B. Hapke, and J. D. Goguen (1988), Photometry and polarimetry of Mercury, in *Mercury*, edited by F. Vilas, C. R. Chapman, and M. S. Matthews, pp. 37–58, Univ. of Arizona Press, Tucson, Ariz.

Vilas, F. (1988), Surface composition of Mercury from reflectance spectrophotometry, in *Mercury*, edited by F. Vilas, C. R. Chapman, and M. S. Matthews, pp. 59–76, Univ. of Arizona Press, Tucson, Ariz.

Warell, J. (2004), Properties of the Hermean regolith: IV. Photometric parameters of Mercury and the Moon contrasted with Hapke modeling, *Icarus*, *167*, 271–286.

Warell, J., and D. T. Blewett (2004), Properties of the Hermean regolith: V. New optical reflectance spectra, comparison with lunar anorthosites, and mineralogical modelling, *Icarus*, *168*, 257–276.

Warell, J., and P. G. Valegård (2006), Albedo-color distribution on Mercury: A photometric study of the poorly known hemisphere, *Astron. Astrophys.*, *460*, 625–633.

Weider, S. Z., L. R. Nittler, R. D. Starr, T. J. McCoy, K. R. Stockstill-Cahill, P. K. Byrne, B. W. Denevi, J. W. Head, and S. C. Solomon (2012), Chemical heterogeneity on Mercury's surface revealed by the MESSENGER X-ray Spectrometer, *J. Geophys. Res.*, *117*, E00L05, doi:10.1029/2012JE004153.

Xiao, Z., et al. (2012), The youngest geologic terrains on Mercury, *Lunar Planet. Sci.*, *43*, abstract 2143.